Research

Fabrication, spectroscopic properties, antioxidant and antimicrobial activities of Chitosan-CaLi@*Flumox* nanocomposites

A. M. Mansour[1] · Mohamed S. Abdel-Aziz[2] · Abdul Aziz M. Gad[3] · Ali B. Abou Hammad[1] · Amany M. El Nahrawy[1]

Received: 8 September 2023 / Accepted: 16 October 2023
Published online: 06 November 2023

Abstract
In the current study, we examined the impact of introducing *Flumox* into the chitosan/calcium lithium (Chitosan-CaLi) nanocomposite on its spectroscopic, thermal, and antimicrobial characteristics. The formation of the nanocomposites was achieved using the sol–gel method/polymerization, which was chosen for its cost-effectiveness and straightforward processing. The UV–Visible optical analysis shows an absorption peak at 290 nm across all samples. Both direct and indirect energy gap types are available where the indirect event exhibits a higher value than the direct transition. There is a noticeable decrease in both transition energies with the increase in *Flumox* content. The findings indicated that as the *Flumox* concentration increased, the Ic_{50} value also increased, signifying a decrease in antioxidant capacity. The results from the obtained systems revealed that chitosan-CaLiO nanoparticles loaded with *Flumox* exhibited remarkable antimicrobial activity, particularly against Pseudomonas aeruginosa and Staphylococcus aureus, demonstrating the highest growth inhibition rate. However, in the case of Aspergillus niger and Candida albicans, the antimicrobial activity was comparatively lower.

Keywords Chitosan composites · CaO nanoparticles · Diffused reflectance · Antimicrobial · Antioxidant

1 Introduction

Chitosan, a cationic biopolymer, possesses noteworthy physicochemical attributes such as non-toxicity, biodegradability, biocompatibility, antibacterial properties, and the ability to form films [1, 2]. These characteristics make it highly relevant in industries such as food, medical, pharmaceutical, agricultural, and optoelectronics. The flexible and permeable film formed by chitosan is a result of its stabilized hydrogen bond network. The blending of biodegradable polymers offers the opportunity to develop a new class of biomaterials with optimized properties tailored for specific applications [3–5]. Furthermore, the incorporation of various ions, nanoparticles, and polymeric materials into chitosan can be achieved using a simple method, thereby expanding its range of applications. Chitosan based bio-polymers generate a new generation of nanomaterials that have tendency to reduce the environmental impact in terms of biomedical, energy consumption and greenhouse effect in specific applications. They are a potential alternative to traditional nanomaterials whose recycling is impossible or not economical [6–8].

Calcium Oxide (CaO) nanoparticles have emerged as a subject of immense interest and research. CaO, commonly known as quicklime, has been an essential compound in various industries for its versatile applications

✉ Ali B. Abou Hammad, abohmad2@yahoo.com; ✉ Amany M. El Nahrawy, amany_physics_1980@yahoo.com | [1]Solid State Physics Department, Physics Research Institute, National Research Centre (NRC), 33 El-Bohouth St., Dokki, Cairo 12622, Egypt. [2]Microbial Chemistry Department, National Research Centre, 33 El Bohouth St., Dokki, Giza 12622, Egypt. [3]Molecular Biology Department, Biotechnology Research Institute, National Research Center, Cairo, Egypt.

[9–11]. These nanoscale entities boast an impressive surface area-to-volume ratio, leading to enhanced reactivity, catalytic efficiency, and novel functionalities. Their exceptional properties open up avenues in fields ranging from materials science and catalysis to medicine and environmental remediation [10, 12, 13]. It is proved that the amalgamation of CaO with silica and phosphate results in exceptional bioactivity, degradability, and biocompatibility. Consequently, this composite holds potential as an alternative material for the restoration of damaged teeth or bones, as well as for applications in drug delivery [9, 14, 15].

Within the field of environmentally conscious systems, the incorporation of LiCa as nanoparticles within the Chitosan-LiCa@*Flumox* framework stands out as an exceptionally enticing objective. This work is driven by the desire to enhance the efficacy of nanocomposites through the integration of diverse functional groups within the polymeric matrix, thus facilitating rapid mass transfer [3–5, 16]. This holds significant value, particularly for versatile applications, making it a matter of considerable importance.

In this study, the copolymerization of chitosan with lithium calcium nanoparticles was employed to produce a positively charged surface and modify the chitosan matrix. An examination was conducted to assess how different ratios of *Flumox* (as a common drug and fast dissolution) influenced the morphology, crystallite degree, thermal properties, and optical characteristics of the resultant nanocomposites. Subsequently, the antioxidant and antimicrobial properties were evaluated to explore their bioactivity. The incorporation of CaLiO nanoparticles into the chitosan matrix, along with loading *Flumox,* resulted in the development of a nanocomposite with outstanding spectroscopic properties for Antioxidant and antimicrobial activities.

2 Expriemental

2.1 Chitosan-CaLi synthesis and loading with *Flumox*

To fabricate the chitosan solution, medium molecular weight (MMW) chitosan from Sigma-Aldrich was used along with acetic acid. The preparation of chitosan involved dissolving 2.3 g of chitosan in 100 ml of a 1 wt.% acetic acid solution. For the synthesis of calcium lithium hydrate in this study, a sol–gel reaction was employed using calcium nitrate (Ca(NO3)2-4H2O) and lithium nitrate (LiNO3- Sigma-Aldrich). Specifically, 20 ml of Ca (NO3)2-4H2O/H2O (Sigma-Aldrich) with a pH of 11.5 and 5 ml of LiNO3 were mixed, followed by stirring the solution for 1 h at 40 ℃. Once complete dissolution of the chitosan and calcium lithium (CaLi) was achieved, the two solutions were combined. The resulting mixture was then cast onto Petri dishes and left to dry at 40 ℃. Finally, loading *Flumox* using separated solution by mixing various doses of *Flumox* with starch-H2O under stirring for 10 min and mixed in the previously prepared chirosan-CaLi solution at room temperature.

2.2 Characterizations

X-ray diffraction (XRD) patterns were collected using a Bruker D8 advance diffractometer with CuKα radiation (λ = 1.540 Å). The instrument operated at 40 kV and 40 mA. Scans were conducted with a detector step size of 0.02°, covering an angular range of 2θ from 10 to 70°.Transmission electron microscope (TEM) images were gotten from (JEOL-2100) microscope -Japan. UV–VIS measurements were recorded using UV/VIS Spectrometer (Lambda 35-PerkinElmer USA). The Tescan Shimadzu FTIR-spectrophotometer (Model 8000, Japan) was used to record FTIR in the range of 400–4000 cm^{-1}. The thermal stability of samples was achieved using a heat heavy difference heat integrated analyzer (Perkin Elmer thermal gravimetric analyzer- TGA7, USA) in the nitrogen atmosphere with a heating rate of 20 ℃ min^{-1}. The UV–visible spectroscopy evaluations were performed using Jasco (V570, USA, UV–vis NIR spectrophotometer).

2.3 Determination of antioxidant capacity

Antioxidants are substances that neutralize reactive oxygen species (ROS) and their actions. Some antimicrobial agents can stimulate the production of ROS as part of their mechanism of action [17]. Therefore, the antioxidant systems of bacterial pathogens could be important to counteract antibiotic ROS production.

The IC_{50} value is a parameter widely used to measure the antioxidant activity of test samples. It is calculated as the concentration of antioxidants needed to decrease the initial DPPH concentration by 50% [18, 19]. Thus, the lower IC_{50} value the higher antioxidant activity.

2.3.1 DPPH free radical scavenging assay

Radical scavenging activity against stable 2, 2 diphenyl 2 picryl hydrazyl hydrate (DPPH) was determined by the slightly modified method of Brand-Williams et al., 1995 [20]. DPPH reacts with an antioxidant compound, which can donate hydrogen, and reduce DPPH. The change in colour (from deep violet to light yellow) was measured at 517 nm on a UV visible light spectrophotometer. The solution of DPPH 0.1 mM in ethanol was prepared fresh daily before UV measurements. The samples were kept in the

dark for 15 min at room temperature and the decrease in absorbance was measured. The experiment was carried out in triplicate. Radical scavenging activity was calculated by the following formula. % Inhibition = $[(A_B - A_A)/A_B] \times 100$ Where A_B = absorption of blank sample (t = 0 min) A_A = absorption of test extract solution (t = 15 min) [20, 21]. The IC_{50} was calculated from the scavenging activities (%) versus concentrations of the respective sample curve.

2.4 Assessment of antimicrobial efficacy

In this section, the antimicrobial activity of the samples was evaluated. The antibacterial activities of chitosan-calcium lithium nanocomposite loaded with (0.1–0.4 wt.%) *Flumox*, were evaluated using the agar plate method. Two bacterial test microorganisms were cultivated on nutrient agar medium (DSMZ1) with the following composition per liter: beef extract (3 g), peptone (10 g), and agar (20 g). The cultures of each microorganism were diluted using sterile distilled water to achieve a concentration of 107–108 CFU/ml (CFU represents the number of cells per ml of the suspension used for inoculation). Polymer-containing discs with a diameter of 10 mm were placed on the surface of the inoculated agar plates (10 cm in diameter with 25 ml of solidified media) and incubated at 37 ℃ for 24 h. For the fungi (Candida albicans), Czapek-Dox or potato dextrose agar was used as the medium, and the incubation time was extended to 48 h at 37 ℃. The obtained results represent the average from duplicate plates.

3 Results and discussion

3.1 XRD

The primary objective of this study revolved around creating nanocomposites based on chitosan, incorporating LiCa nanoparticles with varying proportions of *Flumox*. Hence, the initial phase encompassed the fabrication of uniform LiCa nanoparticles using the sol–gel technique on a nanoscale level, coupled with an in-situ polymerization process. The initial synthesis endeavors concentrated on amalgamating the sol–gel and polymerization methods, a methodology previously documented by our research group. It was observed that this approach yielded nanocomposites exhibiting a degree of crystallinity, leading to the incorporation of LiCa sols within the polymeric matrices.

Figure 1 depicts the X-ray Diffraction (XRD) patterns of chitosan-LiCa nanocomposites loaded with (0.1–0.4 wt.%) of *Flumox*. These profiles align with both the amorphous lithium calcium and chitosan. Analysis of the XRD patterns reveals the emergence of weak peaks, corresponding to

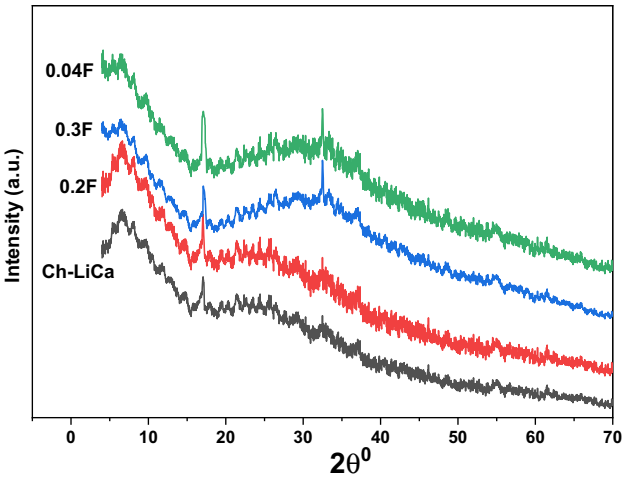

Fig. 1 XRD patterns of chitosan-LiCaO@*Flumox* nanocomposites

the CaO phase and hexagonal calcium hydroxyl phases within the current nanocomposites in the presence of lithium ions [10, 22]. These observations are consistent with the patterns documented in the established standard card (JCPDS card number 37-1497) for CaO. Nevertheless, the chitosan-LiCa@*Flumox* patterns exhibit a broad peak at 6.7° degrees, indicative of a slight increase in breadth along with a reduction in intensity, corresponding to the altered characteristics of chitosan.

3.2 TEM

The TEM image (Fig. 2a) illustrates the morphological characteristics of the CaLi nanoparticles before their incorporation into the chitosan matrix. Upon the formation of the chitosan-CaLi composite and the loading of Flu, the micrograph of the resulting nanocomposite reveals intricate morphological features (Fig. 2b, c). The TEM images of the chitosan-CaLi composite indicate the presence of agglomerated nanoparticles within the polymeric host. With the inclusion of Flu, the agglomeration is observed to increase, accompanied by a predominance of dense-shaped morphology. The diameter of the CaLi nanoparticles in the sample ranges from 3 to 22 nm.

3.3 TGA analysis

Figure 3 presents the thermogram of *Flumox* chitosan-starch/CaLiO nanocomposite with 0 and 0.3 concentration of *Flumox*. It is evident from the thermogram that the weight of samples decreases as the temperature increases. The thermal decomposition of *Flumox* free sample starts at about 192 ℃, while that of 0.3 *Flumox* loading starts at about 40 ℃. Hence, incorporation of *Flumox* into chitosan-starch/CaLiO matrix shifts the onset of

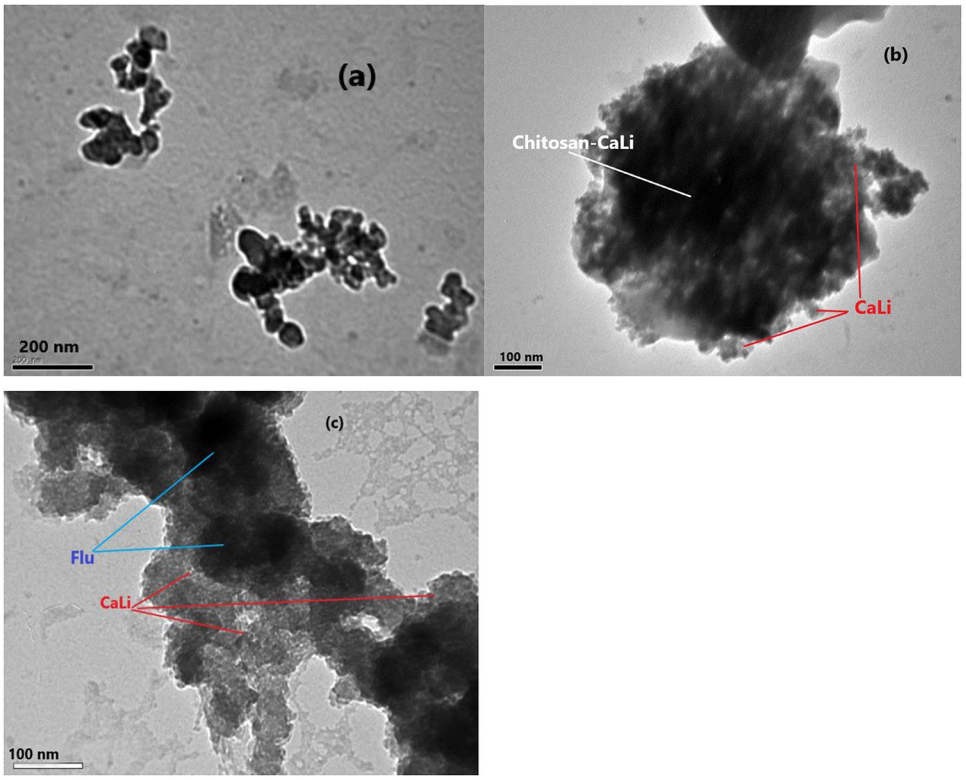

Fig. 2 TEM micrographs of **a** CaLi NPs before mixed in chitosan matrix, **b** Chitosan-CaLi, and **c** loaded with 0.4 *Flumox* nanocomposite

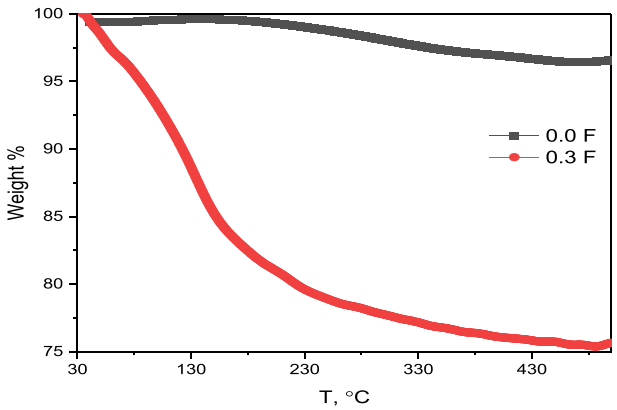

Fig. 3 TGA of chitosan-LiCaO@ *Flumox* nanocomposites

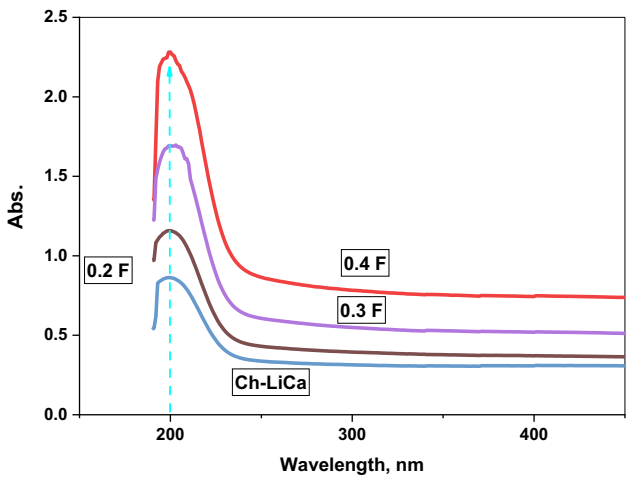

Fig. 4 UV absorption spectra of Chitosan-CaLiO nanocomposite loaded with (0–0.4 wt.%) *Flumox*

thermal decomposition to lower temperature. Moreover, the thermogram reported in Fig. 3 also show that thermal decomposition of the nanocomposites takes place in one step. This step of thermal decomposition (lower temperature region) occurs due to the evaporation of water (solvent) retained in the nanocomposites [23, 24]. After this thermal degradation step, the residual percentage of weight of the nanocomposites left were around 96 and 75% at 500 ℃ for 0 and 0.3 concentration of *Flumox*, respectively. The decrease in residual weight at the end of thermal degradation process is attributed to the presence of *Flumox* in the matrix and the decrease of CaLiO nanoparticles concentration. This shows that addition of *Flumox* decreases the thermal stability of the matrix. Similar results have been quoted by other authors also [25–28].

3.4 *Flumox* loading using Uv-absorbance

Figure 4 presents the UV–Vis absorption spectra of the chitosan-CaLiO nanocomposite loaded with *Flumox* at varying concentrations (0.1–0.4 Wt.%). Initially, the release

study was conducted on samples with the lowest drug ratio of 0.1 for chitosan-CaLiO-0.1 F, in comparison to the unloaded sample. The absorption mechanism involves drug molecules interacting with the CaLi nanoparticles, leading to the formation of drug-CaLi complexes. These complexes result in higher absorbance levels compared to the chitosan-CaLi composite alone. The intricate nature of the nanocomposite also significantly aids in effectively trapping and retaining drugs, further enhancing its drug absorbance capacity. The chitosan-CaLi nanocomposite's ability to absorb drugs at 200 nm offers promising applications in drug delivery systems and pharmaceutical formulations. By capitalizing on this property, researchers and scientists can optimize *Flumox* encapsulation and release processes, potentially advancing targeted therapies and controlled *Flumox* delivery methods.

3.5 Optical properties

Analysis of optical properties of nanocomposites is of huge importance due to their applications in diverse zones such as optical sensors, laser, imaging, solar cell, photocatalysis, etc. [29]. Different optical parameters such as optical energy gap, Urbach's energy, refractive index etc. can be determined with the help of optical characterization [30]. Various factors such as size, shape, nanofillers content and surrounding environment strongly affect the optical properties of nanocomposites. Optical constants of a solid provide the information about its interaction with light [31]. In addition; information about energy band structure, impurity levels, localized defects, etc. of a solid can also be extracted from optical constants [32]. Thus, studies on the effect of increasing concentration of *Flumox* on optical parameters of starch and chitosan loaded with CaLiO are essential for determining their potential applications in different fields.

Figure 5a show the UV–visible absorption spectra of *Flumox* chitosan-starch/CaLiO nanocomposite with varying concentration of *Flumox*. The figure shows that a small values of R for all samples with a semi constant behavior. In the other hand, T have a large value nearly equal to or exceeds 0.8. At about 290 nm, there is a sharp increase of T with wavelength increase for all samples till about 530 nm, where the steady state is reached.

In Fig. 5b, the absorbance changes with wavelength, revealing an absorption peak at 290 nm across all samples. This particular peak, distinguished by its sharp edge, provides evidence of the semicrystalline structure within the Cs-starch-CaLiO matrix [33]. Absorption peak intensities change with *Flumox* addition, confirming component complexation [33].

Optical energy gap of nanocomposites has been calculated using Tauc method [34, 35]. Both direct and indirect energy gap types are available (Fig. 6a, b), and notably, the indirect event exhibits a higher value than the direct transition. As evidenced by Fig. 5c, there is a noticeable decrease in both transition energies with the increase in *Flumox* content. This decrease in Eg values finds its root in the interaction between the organic molecules and inorganic (Ca and Li ions) components [33]. The interaction gives rise to localized states, facilitating the creation of charge transfer complexes between the LUMO and the HOMO [33]. The change in Eg values can be attributed to two significant factors: crosslinking in amorphous regions of CS and an increase in *Flumox*. Consequently, there is

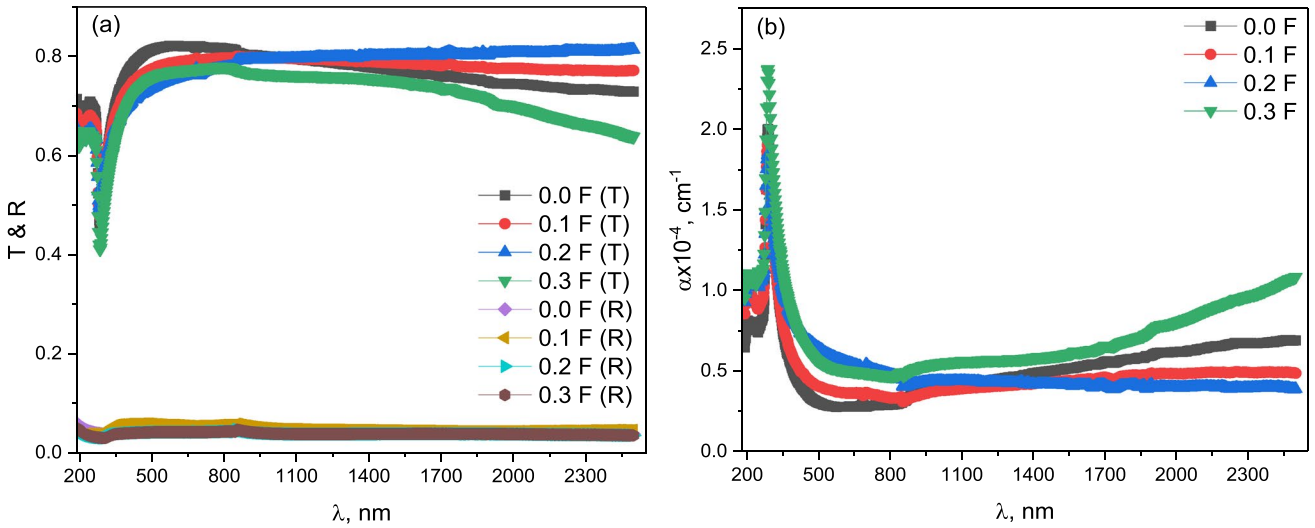

Fig. 5 **a** Transmission and reflection, **b** absorption coefficient of the prepared samples

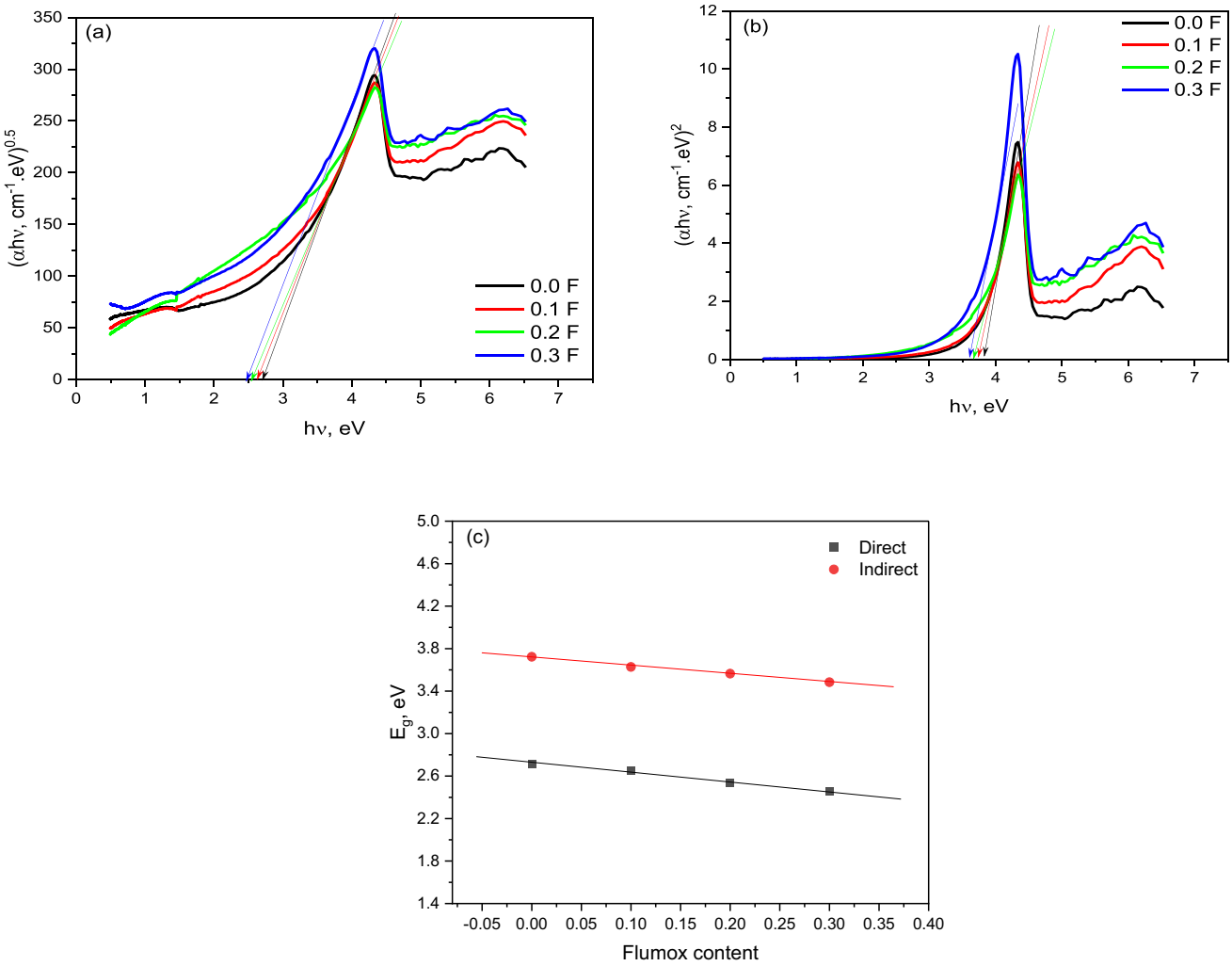

Fig. 6 Tauc relation for **a** direct case, **b** indirect case, and the change of Eg with Flumox content change

a noticeable augmentation of localized states within the forbidden gap [33].

3.6 Antioxidant study

Antioxidants are substances that neutralize reactive oxygen species (ROS) and their actions. Some antimicrobial agents can stimulate the production of ROS as part of their mechanism of action [17]. Therefore, the antioxidant systems of bacterial pathogens could be important to counteract antibiotic ROS production. DPPH assay depends on the measurement of the loss of DPPH free radicals after reaction with test samples. It is considered as the prior mechanism involved in the electron transfer. The IC_{50} value is a parameter widely used to measure the antioxidant activity of test samples. It is calculated as the concentration of antioxidants needed to decrease the initial DPPH concentration by 50% [18, 19]. Thus, the lower IC_{50} value the higher antioxidant activity. The IC_{50} values using DPPH scavenging activity were calculated for different doses of immobilized *Flumox* (Table 1). The results showed that by increasing the *Flumox* concentration, the Ic_{50} increases (antioxidant capacity decreases) and this may be due to the loading capacity of chitosan/gelatin support which

Table 1 Antioxidant capacity for chitosan/gelatin using DPPH method

Flumox (g)	Ic_{50} (µg Flumox/ml)
0.0F	59 ± 0.7
0.1F	188 ± 2
0.2F	285.7 ± 13
0.3F	512 ± 20

Values are presented as mean ± SD from n = 3–4 independent experiments

gives its maximum antioxidant capacity with the dose of 0.1 g *Flumox* [19].

Table 2 showed that the 4Li has a powerful antioxidant capacity compared to the 0Li and 2Li mole ratio where by increasing *Flumox* mole ratio, the antioxidant capacity increases (Ic_{50} decreases). Indeed, active hydroxyl groups in chitosan backbone play an important role in scavenging of DPPH free radicals than the amino ones**.** Moreover, it is well known that chitosan has strong intra- and intermolecular hydrogen bonds consequently, OH is difficult to dissociate [19].

3.7 Antimicrobial activity

The antimicrobial activities of the treated fabrics were assessed using the disc agar plate method. To evaluate the antimicrobial activities of the treated fabrics, four different test microbes were selected: Staphylococcus aureus (representing Gram-positive bacteria), Escherichia coli (representing Gram-negative bacteria), Candida albicans (representing yeast), and Aspergillus niger (representing fungi). The bacterial and yeast test microbes were cultured on a nutrient agar medium (DSMZ1) consisting of peptone (5.0 g), meat extract (3.0 g), agar (20.0 g), distilled water (1000.0 ml), and adjusted to a pH of 7.0. On the other hand, the fungal test microbe was cultivated on Czapek-Dox medium (DSMZ130) containing sucrose (30.00 g), NaNO3 (3.0 g), MgSO4 × 7 H2O (0.50 g), KCl (0.50 g), FeSO4 × 7 H2O (0.01 g), K2HPO4 (1.0 g), agar (18.0 g), distilled water (1000.0 ml), and adjusted to a pH of 7.2.

The cultures of each test microbe were diluted using sterilized distilled water to achieve a concentration of approximately 107–108 cells/ml. Subsequently, 1 ml of each diluted culture was used to inoculate a 1L Erlenmeyer flask containing 250 ml of solidified agar media. These media were then transferred to pre-sterilized Petri dishes (10 cm in diameter) containing 25 ml of solidified media. The treated fabric discs with a diameter of 10 mm were placed on the surface of the agar plates that were seeded with the respective test microbes. The plates were incubated for 24 h at the appropriate temperature for each test organism. The antimicrobial activities were recorded as the diameter of the clear zones (including the film itself) that appeared around the fabric discs as predicted in Table 3. By synthesizing the chitosan-CaLi/Flumox nanocomposite, the controlled release of CaLiO nanoparticles and Flu is achieved, offering an effective solution to prevent and inhibit the proliferation of harmful microbes. The CaLiO nanoparticles exhibit the capability to interact with microbes, forming strong bonds with their cellular enzymes, thereby effectively impeding enzyme activity and suppressing microbial growth (Fig. 7). This interaction eventually results in the eradication of the microbes.

Table 2 Antioxidant capacity for chitosan/starch/CaLio using DPPH method

Sample	Ic_{50} (mmol CaLiO/ml)
0F	63 ± 2
0.2F	12.5 ± 0.25
0.3F	4 ± 0.03

Values are presented as mean ± SD from n = 3–4 independent experiments

4 Conclusion

The monomodal LiCa nanoparticles enriched with Flumox and their integration into chitosan nanocomposites was synthesized employing sol–gel and polymerization methodologies. Our observations indicated an increase in crystallinity within these materials, accompanied by a decreased in the bandgap as well as a decrease in thermal stability as the Flumox content increased. In conclusion,

Table 3 Microbial sensitivity of samples loaded with Flumox-nanocomposite against pathogenic verified microorganisms

Sample name	Clear zone (ϕmm)			
	Staphylococcus aureus	*Pseudomonas aeruginosa*	*Candida albicans*	*Aspergillus niger*
Ch-LiCa	13	14	14	11
Ch-LiCa-0.2 CL	11	11	11	11
Ch-LiCa-0.3 Cl	15	13	14	13
Ch-LiCa-0.4 CL	15	15	14	14

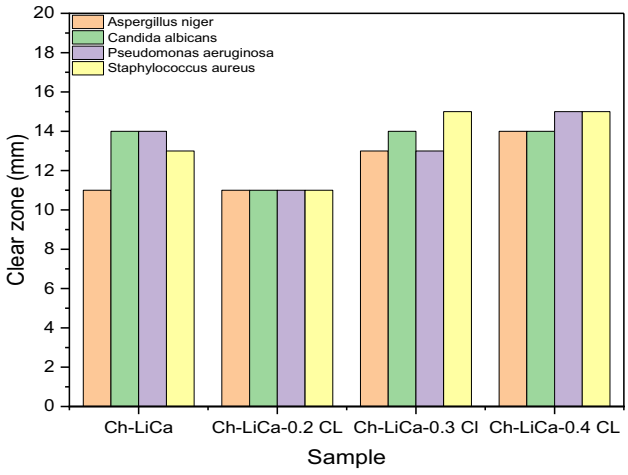

Fig. 7 Antimicrobial activates of chitosan-LiCaO@ *Flumox* nanocomposites

chitosan-copper demonstrates notable drug absorbance at 200 nm due to its unique interaction with drug molecules and CaLiO NPs. This characteristic opens up possibilities for innovative drug delivery approaches and holds promise for improving drug efficacy. An absorption peak at 290 nm across all samples was observed, and distinguished by its sharp edge, provides evidence of the semicrystalline structure within the Cs-starch-CaLiO matrix. A noticeable decrease in both direct and indirect transition energies with the increase in Fumox content. This decrease in Eg values finds its root in the interaction between the chitosan/Flumox and inorganic (Ca and Li ions) components which generate localized states within the forbidden gap.

Author contributions All authors wrote the main manuscript and reviewed their parts and the manuscript

Funding Open access funding provided by The Science, Technology & Innovation Funding Authority (STDF) in cooperation with The Egyptian Knowledge Bank (EKB).

Data availability Data will be made available on request.

Declarations

Conflict of interest The authors declare no competing interests.

References

1. Attayil Sukumaran S, Kalimuthu B, Selvamurugan N, Mani P (2022) Wound dressings based on chitosan/gelatin/MgO composite films. Int J Polym Mater Polym Biomater 71:1252–1261. https://doi.org/10.1080/00914037.2021.1960342
2. Martínez-Camacho AP, Cortez-Rocha MO, Ezquerra-Brauer JM et al (2010) Chitosan composite films: thermal, structural, mechanical and antifungal properties. Carbohydr Polym 82:305–315. https://doi.org/10.1016/J.CARBPOL.2010.04.069
3. Abou Hammad AB, Al-esnawy AA, Mansour AM, El Nahrawy AM (2023) Synthesis and characterization of chitosan-corn starch-SiO2/silver eco-nanocomposites: exploring optoelectronic and antibacterial potential. Int J Biol Macromol 249:126077. https://doi.org/10.1016/J.IJBIOMAC.2023.126077
4. Paunova-Krasteva T, Hemdan BA, Dimitrova PD et al (2022) Hybrid Chitosan/CaO-Based nanocomposites doped with plant extracts from Azadirachta indica and Melia azedarach: evaluation of antibacterial and antibiofilm activities. Bionanoscience. https://doi.org/10.1007/s12668-022-01047-0
5. Chen W, Yue L, Jiang Q et al (2018) Synthesis of varisized chitosan-selenium nanocomposites through heating treatment and evaluation of their antioxidant properties. Int J Biol Macromol 114:751–758. https://doi.org/10.1016/j.ijbiomac.2018.03.108
6. Cano A, Cháfer M, Chiralt A, González-Martínez C (2016) Development and characterization of active films based on starch-PVA, containing silver nanoparticles. Food Packag Shelf Life 10:16–24. https://doi.org/10.1016/j.fpsl.2016.07.002
7. Farhoudian S, Yadollahi M, Namazi H (2016) Facile synthesis of antibacterial chitosan/CuO bio-nanocomposite hydrogel beads. Int J Biol Macromol 82:837–843. https://doi.org/10.1016/j.ijbiomac.2015.10.018
8. Adsorption of phenol on environmentally friendly Fe_3O_4/ chitosan/ zeolitic imidazolate framework-8 nanocomposite: optimization by experimental design methodology. https://www.researchgate.net/publication/347518555_Adsorption_of_phenol_on_environmentally_friendly_Fe3O4_chitosan_zeolitic_imidazolate_framework-8_nanocomposite_Optimization_by_experimental_design_methodology. Accessed 11 Oct 2021
9. El Nahrawy A, Bakr A, AbouHammad A, Mansour AF (2021) Nano-architecture of CaO/Ag-chitosan nanocomposite by sol gel process: formation and characterization. Egypt J Chem 64:7393–7406. https://doi.org/10.2160/ejchem.2021.80608.3995
10. Mirghiasi Z, Bakhtiari F, Darezereshki E, Esmaeilzadeh E (2014) Preparation and characterization of CaO nanoparticles from Ca(OH)2 by direct thermal decomposition method. J Ind Eng Chem 20:113–117. https://doi.org/10.1016/j.jiec.2013.04.018
11. Sharifianjazi F, Parvin N, Tahriri M (2017) Synthesis and characteristics of sol-gel bioactive SiO2-P2O5-CaO-Ag2O glasses. J Non Cryst Solids 476:108–113. https://doi.org/10.1016/J.JNONCRYSOL.2017.09.035
12. Kaur P, Singh KJ, Yadav AK et al (2018) Preliminary investigation of the effect of doping of copper oxide in CaO-SiO2-P2O5-MgO bioactive composition for bone repair applications. Mater Sci Eng C 83:177–186. https://doi.org/10.1016/j.msec.2017.09.006
13. Kaur K, Singh KJ, Anand V et al (2016) Magnesium and silver doped CaO–Na2O–SiO2–P2O5bioceramic nanoparticles as implant materials. Ceram Int. https://doi.org/10.1016/j.ceramint.2016.05.001
14. Abou Hammad AB, Elnahrawy AM, Youssef AM, Youssef AM (2019) Sol gel synthesis of hybrid chitosan/calcium aluminosilicate nanocomposite membranes and its application as support for CO_2 sensor. Int J Biol Macromol 125:503–509. https://doi.org/10.1016/j.ijbiomac.2018.12.077
15. ElNahrawy AM, AbouHammad AB (2016) A facile co-gelation sol gel route to synthesize CaO: P_2O_5: SiO_2 xerogel embedded in chitosan nanocomposite for bioapplications. Int J Pharmtech Res 9:16–21
16. Tripathi S, Mehrotra GK, Dutta PK (2011) Chitosan–silver oxide nanocomposite film: preparation and antimicrobial activity. Bull Mater Sci 34:29–35. https://doi.org/10.1007/s12034-011-0032-5
17. Kim SY, Park C, Jang HJ et al (2019) Antibacterial strategies inspired by the oxidative stress and response networks. J Microbiol 57:203–212. https://doi.org/10.1007/S12275-019-8711-9
18. Zhai L, Bai Z, Zhu Y et al (2018) Fabrication of chitosan microspheres for efficient adsorption of methyl orange. Chin J Chem Eng 26:657–666. https://doi.org/10.1016/J.CJCHE.2017.08.015
19. Rivero-Cruz JF, Granados-Pineda J, Pedraza-Chaverri J et al (2020) Phytochemical constituents, antioxidant, cytotoxic,

and antimicrobial activities of the ethanolic extract of Mexican brown propolis. Antioxidants 9:70. https://doi.org/10.3390/ANTIOX9010070
20. dos Santos PA, Peixoto CN, de Souza VCP et al (2023) Analytical and chemometric strategies for elucidation of yerba mate composition. Food Chem. https://doi.org/10.1016/j.foodchem.2023.136918
21. Brand-Williams W, Cuvelier ME, Berset C (1995) Use of a free radical method to evaluate antioxidant activity. LWT Food Sci Technol 28:25–30. https://doi.org/10.1016/S0023-6438(95)80008-5
22. Madhu BJ, Bhagyalakshmi H, Shruthi B, Veerabhadraswamy M (2021) Structural, AC conductivity, dielectric and catalytic behavior of calcium oxide nanoparticles derived from waste eggshells. SN Appl Sci. https://doi.org/10.1007/S42452-021-04607-3
23. El-Menyawy EMM, Mansour AMM, El-Ghamaz NAA, El-Khodary SAA (2013) Electrical conduction mechanisms and thermal properties of 2-(2, 3-dihydro-1,5-dimethyl-3-oxo-2-phenyl-1H-pyrazol-4-ylimino)-2-(4-nitrophenyl) acetonitrile. Phys B Condens Matter 413:31–35. https://doi.org/10.1016/j.physb.2012.12.030
24. El-Menyawy EMM, Zedan ITT, Mansour AMM et al (2014) Thermal stability, AC electrical conductivity and dielectric properties of N-(5-{[antipyrinyl-hydrazono]-cyanomethyl}-[1,3,4]thiadiazol-2-yl)-benzamide. J Alloys Compd 611:50–56. https://doi.org/10.1016/j.jallcom.2014.05.120
25. Jiménez-Regalado EJ, Caicedo C, Fonseca-García A et al (2021) Preparation and physicochemical properties of modified corn starch-chitosan biodegradable films. Polymers (Basel). https://doi.org/10.3390/POLYM13244431
26. Cárdenas G, Miranda SP (2004) FTIR and TGA studies of chitosan composite films. J Chil Chem Soc 49:291–295. https://doi.org/10.4067/S0717-97072004000400005
27. Ashori A, Bahrami R (2014) Modification of physico-mechanical properties of Chitosan-Tapioca starch blend films using nano graphene. Polym Plast Technol Eng 53(3):312–318. https://doi.org/10.1080/03602559.2013.866246
28. Aguirre-Loredo RY, Fonseca-García A, Calambas HL et al (2023) Improvements of thermal and mechanical properties of achira starch/chitosan/clay nanocomposite films. Heliyon. https://doi.org/10.1016/J.HELIYON.2023.E16782
29. El Nahrawy AM, Abou Hammad AB, Mansour AM (2021) Compositional effects and optical properties of P2O5 doped magnesium silicate mesoporous thin films. Arab J Sci Eng 46:5893–5906. https://doi.org/10.1007/s13369-020-05067-4
30. El Nahrawy AM, Hemdan BA, Mansour AM et al (2021) Integrated use of nickel cobalt aluminoferrite/Ni2+ nano-crystallites supported with SiO2 for optomagnetic and biomedical applications. Mater Sci Eng B Solid State Mater Adv Technol 274:115491. https://doi.org/10.1016/j.mseb.2021.115491
31. Hassan N, Mansour AM, Roushdy N et al (2018) Optical sensing performance characteristics of Schottky devices diodes based nano-particle disodium 6-hydroxy-5-[(2-methoxy-5-methyl-4-sulfophenyl)azo]-2-naphthalenesulfonate thin films: a comparison study. Optik (Stuttg) 158:1255–1265. https://doi.org/10.1016/j.ijleo.2017.12.203
32. Farag AAM, Terra FS, Ashery A, Mansour AM (2014) Structural and electrical characteristics of n-InSb/p-GaAs heterojunction prepared by liquid phase epitaxy. J Alloys Compd 615:604–609. https://doi.org/10.1016/j.jallcom.2014.06.058
33. Gaabour LH (2019) Influence of silica nanoparticles incorporated with chitosan/polyacrylamide polymer nanocomposites. J Market Res 8:2157–2163. https://doi.org/10.1016/J.JMRT.2019.02.003
34. El Nahrawy AM, Mansour AM, Abou Hammad AB, Wassel AR (2019) Effect of Cu incorporation on morphology and optical band gap properties of nano-porous lithium magneso-silicate (LMS) thin films. Mater Res Express 6:016404. https://doi.org/10.1088/2053-1591/aae343
35. Mansour AM, Abou Hammad AB, Bakr AM, El Nahrawy AM (2022) Silica zinc titanate wide bandgap semiconductor nanocrystallites: synthesis and characterization. Silicon 14:11715–11729. https://doi.org/10.1007/s12633-022-01886-2